PROCEEDINGS OF SCIENCE

Particle Production in p-p and Heavy Ion Collisions at Ultrarelativistic Energies.

J. Cleymans[*a], **S. Kabana**[b], **I. Kraus**[c], **H. Oeschler**[d,e], **K. Redlich**[f], **N. Sharma**[e,g]

[a] *UCT-CERN Research Centre and Department of Physics, University of Cape Town, Rondebosch 7701, South Africa*

[b] *SUBATECH, 4 rue Alfred Kastler, F-44307 Nantes, France*

[c] *GSI, Planckstrasse 1, D-64291 Darmstadt, Germany*

[d] *Institut für Kernphysik, Darmstadt University of Technology, D-64289 Darmstadt, Germany*

[e] *European Organization for Nuclear Research (CERN), Geneva, Switzerland*

[f] *Institute of Theoretical Physics, University of Wrocław, Pl-45204 Wrocław, Poland*

[g] *Department of Physics, Panjab University, Chandigarh, India*

Recent results related to the chemical equilibration of hadrons in the final state of p-p and heavy ion collisions are reviewed.

Kruger2010: Workshop on Discovery Physics at the LHC,
December 5 - 10 2010
Kruger National Park, South Africa

[*] Speaker.

PoS(Kruger 2010)043

1. Introduction

After analysing particle multiplicities for two decades a remarkably simple picture has emerged for the chemical freeze-out parameters [1, 2, 3]. Despite much initial skepticism, the thermal model

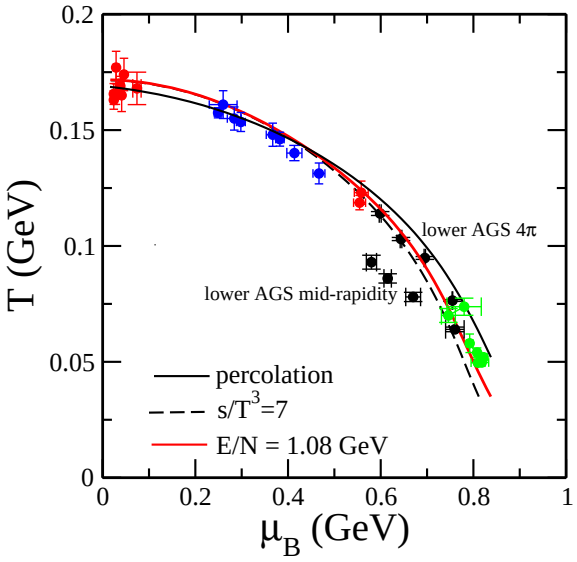

Figure 1: Values of the freeze-out parameters obtained at beam energies ranging from 1 GeV to 200 GeV

has emerged as a reliable guide for particle multiplicities in heavy ion collisions at all collision energies. Some of the results, including analyses from [4, 5, 6, 7], are summarised in Fig. 1. Most of the points in Fig. 1 (except obviously the ones at RHIC) refer to integrated (4π) yields. A clear discrepancy exists in the lower AGS beam energy region between the chemical parameters extracted from (published) mid-rapidity yields and those extracted using estimates of the 4π yields. The latter tend to give higher values for the chemical freeze-out temperature. This will have to be resolved by future experiments at e.g. NICA and FAIR. When the temperature and baryon chemical potential are translated to net baryon and energy densities, a different, but equivalent, picture emerges shown in Fig. 2. This clearly shows the importance in going to the beam energy region of around 8 - 12 GeV as this corresponds to the highest freeze-out baryonic density and to a rapid change in thermodynamic parameters [8, 9].

The dependence of μ_B on the invariant beam energy, $\sqrt{s_{NN}}$, can be parameterized as [3]

$$\mu_B(\sqrt{s_{NN}}) = \frac{1.308 \text{ GeV}}{1 + 0.273 \text{ GeV}^{-1} \sqrt{s_{NN}}}.$$

Similar dependences have been obtained by other groups [1, 2]. and are consistent with the above. This predicts that at the LHC $\mu_B \approx 1$ MeV.

To analyze the changes around 10 GeV use can be made of the entropy density, s, divided by T^3 which has been shown to reproduce the freeze-out curve [3] very well. This allows for a separation into baryonic and mesonic components, shown in Fig. 3, it can be seen that mesons dominate the chemical freeze-out from about $\sqrt{s_{NN}} \approx 10$ GeV onwards.

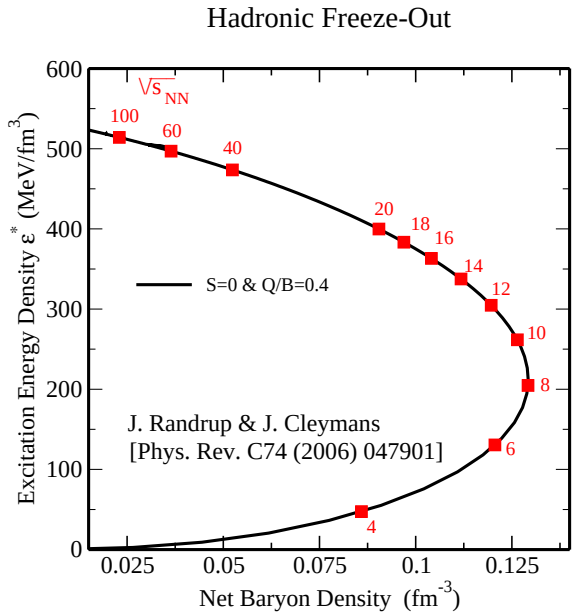

Figure 2: The hadronic freeze-out line in the $\rho_B - \varepsilon^*$ phase plane as obtained from the values of μ_B and T that have been extracted from the experimental data in [3]. The calculation employs values of μ_Q and μ_S that ensure $\langle S \rangle = 0$ and $\langle Q \rangle = 0.4 \langle B \rangle$ for each value of μ_B. Also indicated are the beam energies (in GeV/N) for which the particular freeze-out conditions are expected at either RHIC or FAIR or NICA.

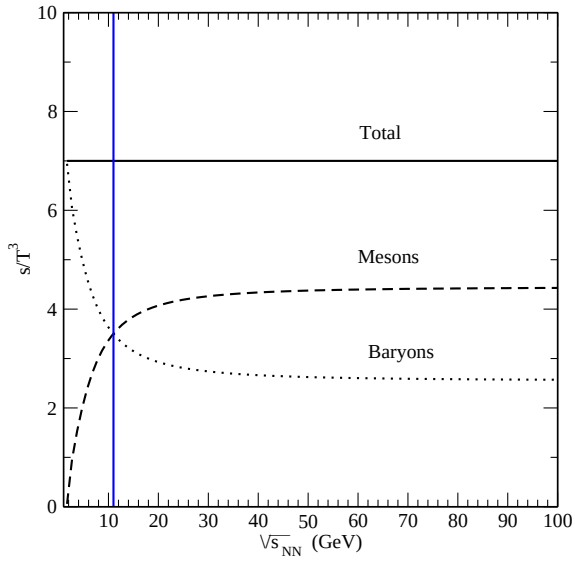

Figure 3: Values of entropy density divided by T^3 following the chemical freeze-out values [10].

2. Antimatter Production

One of the striking features of particle production at high energies is the near equal abundance of matter and antimatter in the central rapidity region [11, 12]. As is well known a similar symmetry existed in the initial stage of the universe and it still remains a mystery as to how this got lost in the evolution of the universe reaching a stage with no visible amounts of antimatter being present. Closely related to this matter/antimatter symmetry is the production of light antinuclei, hypernuclei and antihypernuclei at high energies. Since the first observation of hypernuclei in 1952 [13] there has been a steady interest in searching for new hypernuclei and exploring the hyperon-nucleon interaction which is relevant (see e.g. [14, 15]) for nuclear physics. Hypernuclei decay with lifetime which depends on the strength of the hyperon-nucleon interaction. While several hypernuclei have been discovered since the first observations in 1952, no antihypernucleus has ever been observed until the recent discovery of the antihypertriton in Au+Au collisions at $\sqrt{s_{NN}}$ = 200 GeV by the STAR collaboration at RHIC [16]. The yield of (anti)hypernuclei measured by STAR is very large, in particular they seem to be produced with a similar yield as other (anti)nuclei, in particular (anti)helium-3. This abundance is much higher than measured for hypernuclei and nuclei at lower energies [17]. It is of interest to understand the nature of this enhancement, and for this the mechanism of production of (anti)hypernuclei should be investigated.

The analysis of particle production assessing the degree of thermalization of the particle source has been undertaken for many decades [18, 19, 20, 21, 22]. It has been found that the thermalization assumption applies successfully to hadrons produced in a large number of particle and nuclear reactions at different energies [23, 24]. This fact allows us to estimate thermal parameters characterizing the particle source for each colliding system, relevant for the understanding of the thermal properties of dense and hot matter, and in particular for studies of QCD phase transitions. In this paper, using the parametrizations of thermal parameters estimated by the model THERMUS [25, 26] that were shown to best fit the existing data from particle and nuclear collisions at several energies, we make thermal model estimates of (anti)hypernuclei that can be directly compared to the recently measured unexpected high (anti)hypernuclei yields at RHIC as well as predictions of (anti)matter and (anti)hypernuclei production at the Large Hadron Collider (LHC). A similar analysis, not including p-p results, has been presented recently in [27] where it was shown that ratios of hypernuclei to nuclei show an energy dependence similar to the K^+/π^+ one with a clear maximum at lower energies. In this paper we study quantitatively how the matter/antimatter symmetry is reached as the beam energy is increased. We also estimate ratios of hypernuclei and antihypernuclei yields in Au+Au collisions at RHIC using the above mentioned parametrizations of thermal parameters that best fit hadron production at RHIC. The present analysis uses a thermal model and aims to elucidate the production mechanism of hypernuclei and antihypernuclei in heavy ion collisions at RHIC and LHC energies, thus providing insight in the surprising increase of (anti)hypernuclei production at high energies.

3. The THERMUS model

The thermal model assumes that at freeze-out all hadrons in the hadron gas resulting from a high energy collision follow equilibrium distributions. The conditions at chemical freeze-out

(when inelastic collisions cease) are given by the hadron abundances, while the particle spectra offer insight into the conditions at thermal freeze-out (when elastic collisions cease). Once evaluated the hadron gas partition function gives all primordial thermodynamic quantities of the system by simple differentiation. The exact form of the partition function, however, depends on the statistical ensemble under consideration.
Within the grand-canonical ensemble the quantum numbers of the system are conserved on average through the action of chemical potentials [23]. In other words, the baryon content B, strangeness content S and charge content Q are fixed on average by μ_B, μ_S and μ_Q respectively. For each of these chemical potentials one can write a corresponding fugacity using the standard prescription $\lambda = e^{\mu/T}$, where T is the temperature of the system.

As an example, the density of hadron species i with quantum numbers B_i, S_i and Q_i, spin-isospin degeneracy factor, g_i, and mass, m_i, emitted directly from the fireball at temperature T is given by a second order modified Bessel function of the second kind,

$$\tilde{n}_i(T,\mu_B,\mu_S,\mu_Q,\gamma_S) = \frac{g_i}{2\pi^2} m_i^2 T \lambda_B^{B_i} \lambda_S^{S_i} \lambda_Q^{Q_i} \gamma_s^{|\tilde{S}_i|} K_2(\frac{m_i}{T}). \tag{3.1}$$

in the Boltzmann approximation.
The quantum-statistical result requires either an infinite summation over such K_2 functions or else a numerical integration [25, 26].

The chemical potentials μ_S and μ_Q are typically constrained in applications of the model by the initial strangeness and baryon-to-charge ratio in the system under consideration.

4. Production of antibaryons

In heavy-ion collisions the increase in the antimatter to matter ratio with the center-of-mass energy of the system has been observed earlier by the NA49 [28, 29] and the STAR [30] collaborations. The trend of $\bar{\text{p}}$/p ratio increase with the energy towards unity is shown in Fig. 4, where the open squares refer to heavy ion collisions and the solid circles refer to p-p collisions. It include results from the NA49 [28], STAR [30] and the new results from the ALICE Collaboration [12]. The resulting baryon chemical potential μ_B is shown in Fig. 5 where the dashed line refers to the heavy ion description using the THERMUS model [25, 26]. The two input parameters, the chemical freeze-out temperature T and the baryon chemical potential μ_B as a function of $\sqrt{s}$ are taken from Ref. [31].

$$T(\mu_B) = a - b\mu_B^2 - c\mu_B^4 \tag{4.1}$$

with $a = 0.166 \pm 0.002$ GeV, $b = 0.139 \pm 0.016$ GeV^{-1} and $c = 0.053 \pm 0.021$ GeV^{-3}. This parametrization is similar and consistent with the one proposed in Ref. [33]. The solid line in Fig. 4 is obtained from THERMUS model [25, 26] using T from equation 1 and μ_B from equation 2. The solid circles represent μ_B, obtained after fitting experimental data with the THERMUS model [25, 26]. The solid line is a new parametrization adjusted for pp collisions. In view of the fact that peripheral and central collisions show no noticeable change in the temperature we have

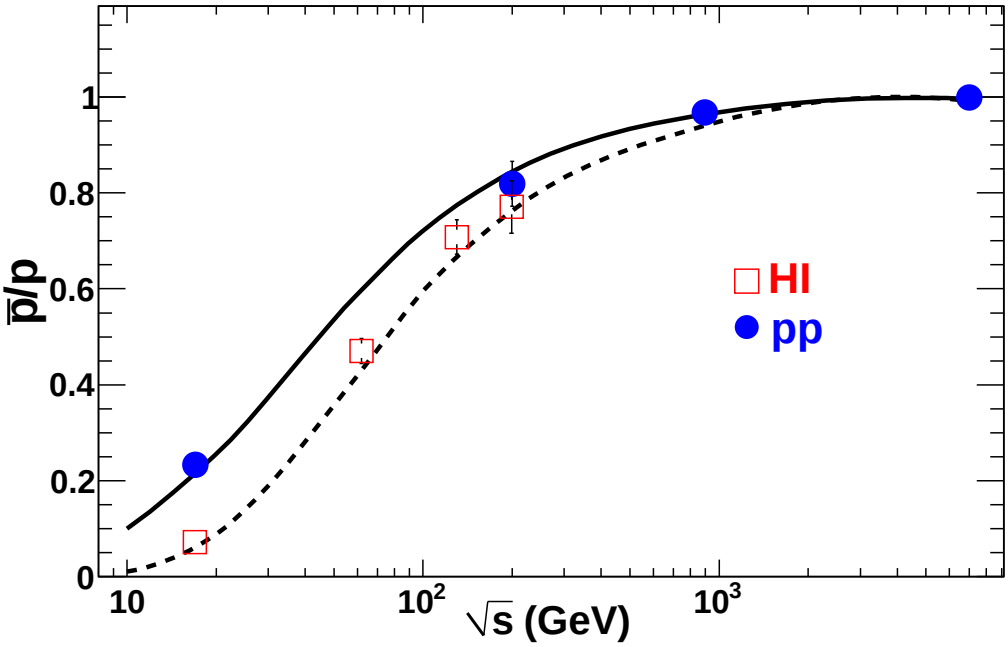

Figure 4: The $\bar{\mathrm{p}}$/p ratio as function of $\sqrt{s}$. The solid circles are results from p-p collisions and the open squares are results from HI collisions as a function of the invariant beam energy[28, 30, 12, 29, 11].

used the same T dependence for p-p as in heavy ion collisions but the dependence on μ_B on beam energy is now given by

$$\mu_B = d/(1+e\sqrt{s}) \tag{4.2}$$

with d = 0.4 GeV and $e = 0.1599$ GeV^{-1}.

It is important to note that μ_B is always lower in pp collisions than in heavy ion collisions, e.g. the freeze-out chemical potential follows a different pattern, due to the lower stopping power in pp collisions.

The relation between the $\bar{\mathrm{p}}$/p ratio and μ_B can be shown easily within the statistical concept using the Boltzmann statistics Ref. [32]. In the model calculation, the appropriate statistics and also feed down from strong decays are taken into account. The density of particle i is then given by

$$n_i = \frac{d_i}{2\pi^2} K_2\left(\frac{m_i}{T}\right) e^{(N_B\mu_B + N_S\mu_S)/T} \tag{4.3}$$

with N_B and N_S being the baryon and strangeness quantum numbers of particle i.

This leads to a $\bar{\mathrm{p}}$/p ratio of (excluding feed-down from heavier resonances):

$$\frac{n_{\bar{\mathrm{p}}}}{n_{\mathrm{p}}} = e^{-(2\mu_B)/T} \tag{4.4}$$

The ratio of strange antibaryons/ baryons is then given by

$$\frac{n_{\bar{\mathrm{B}}}}{n_{\mathrm{B}}} = e^{-(2\mu_B - N_S\mu_S)/T} \tag{4.5}$$

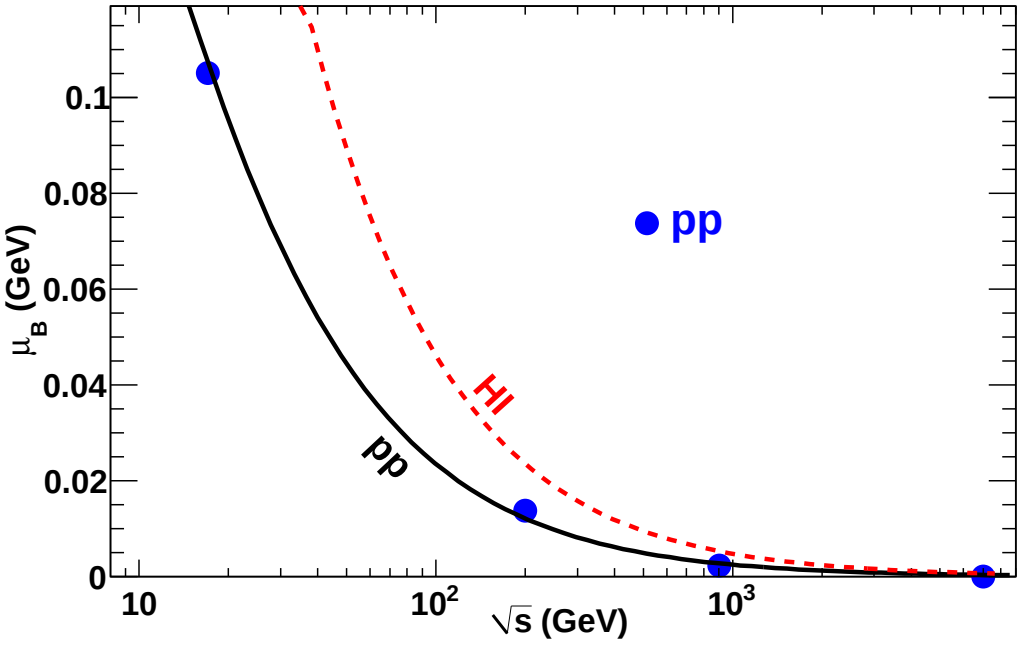

Figure 5: Variation of the baryon chemical potential μ_B as a function of $\sqrt{s}$. The dashed line describes heavy ion collisions as in Ref. [31] while the solid line is the new parametrization for pp collisions.

As μ_S is always smaller than μ_B, the ratios appear ordered with the strangeness quantum number, i.e. the higher N_S, the smaller the difference between antibaryon and baryon. This trend is shown in Figs. 6 and 7 comparing the results from the model with experimental data. The agreement between the model results and the data is very good.

5. Production of nuclei, antinuclei, hypernuclei and antihypernuclei

5.1 Comparison to data from RHIC

The production of light nuclei including hypertritons ($^3_\Lambda$H) and antihypertritons ($^3_{\overline{\Lambda}}\overline{\text{H}}$) was recently observed by the STAR collaboration [16]. The abundances of such light nuclei and antinuclei follows a consistent pattern in the thermal model. The temperature remains the same as before but an extra factor of μ_B is picked up each time the baryon number is increased. Each proton or neutron thus simply adds a factor of μ_B to the Boltzmann factor. The production of nuclear fragments is therefore very sensitive to the precise value of the baryon chemical potential and could thus lead to a precise determination of μ_B.

The ratios within the statistical approach using the grand-canonical formalism can be easily written, based on Eq. (4.3). Deuterium has an additional neutron and the antideuterium to deuterium ratio is given by the square of the antiproton to prton ratio:

$$\frac{n_{\overline{\text{d}}}}{n_{\text{d}}} = e^{-(4\mu_B)/T} \tag{5.1}$$

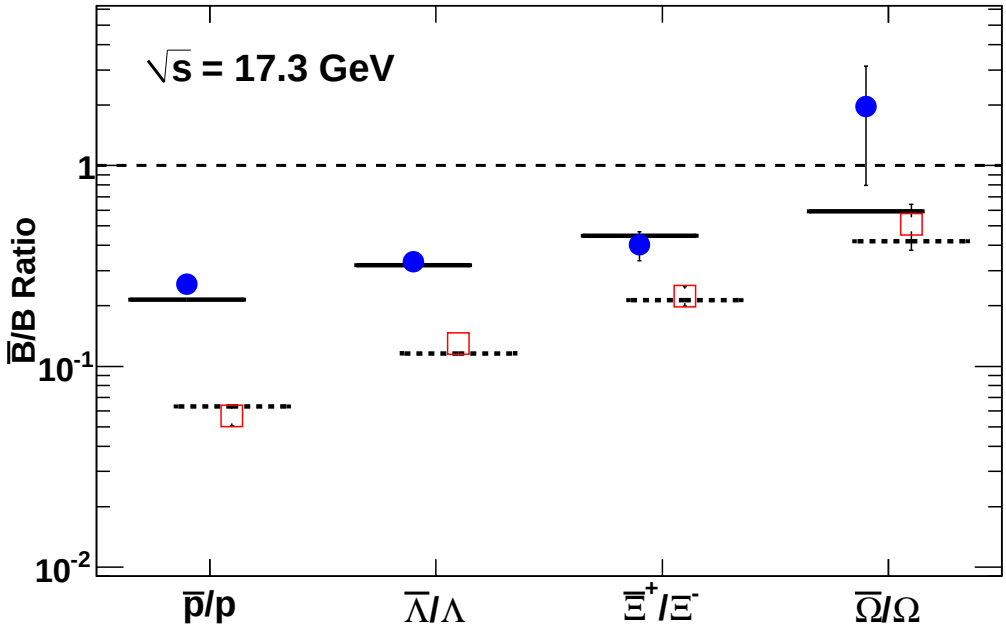

Figure 6: Antibaryon to baryon ratios at the SPS according to strangeness content. Circles refer to p-p collisions, squares to heavy ion collisions.

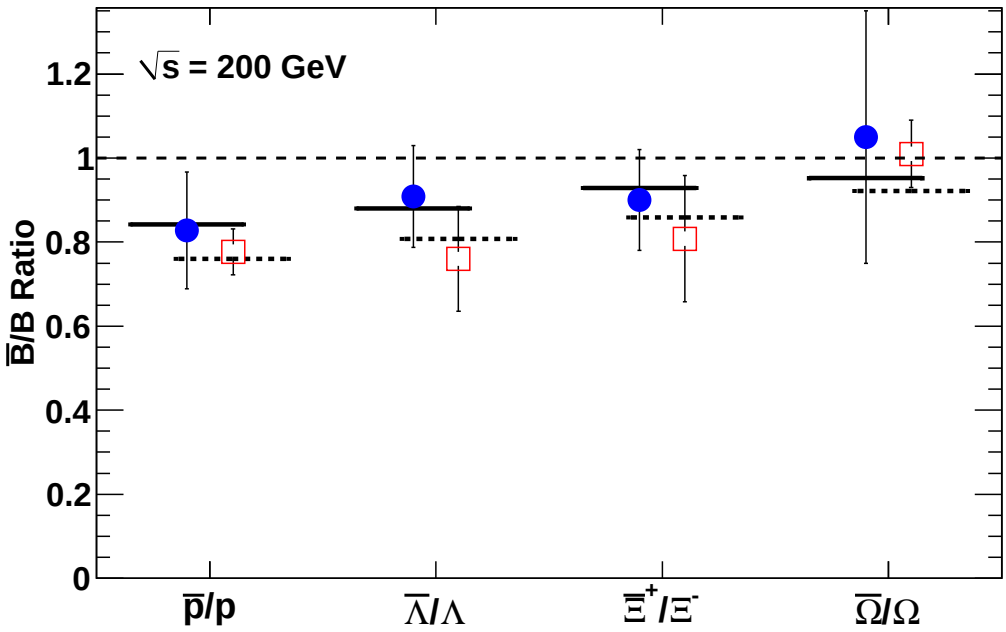

Figure 7: Antibaryon to baryon ratios at STAR according to strangeness content. Circles refer to p-p collisions, squares to heavy ion collisions.

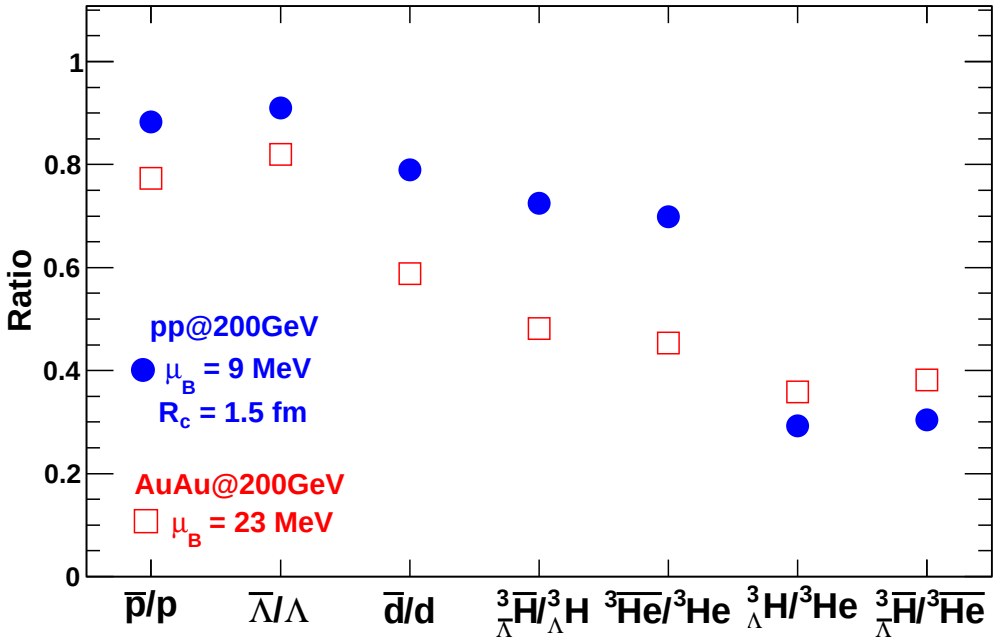

Figure 8: Comparison of pp and heavy ion collisions at $\sqrt{s}$= 200 GeV evidencing the influence of different values of μ_B and of the canonical suppression.

Helium 3 has 3 nucleons and the corresponding anti-Helium 3 to helium 3 ratio is given by:

$$\frac{n_{^3\overline{\rm He}}}{n_{^3{\rm He}}} = e^{-(6\mu_B)/T} \tag{5.2}$$

If the nucleus carries strangeness this leads to an extra factor of μ_S

$$\frac{n_{^3_{\overline{\Lambda}}\overline{\rm H}}}{n_{^3_{\Lambda}{\rm H}}} = e^{-(6\mu_B-2\mu_S)/T} \tag{5.3}$$

In mixed ratios the different degeneracy factors are also taken into account, e.g. 6 for ${}^3_{\Lambda}H$ and 2 for ${}^3_{\Lambda}H$.

$$\frac{n_{^3_{\Lambda}{\rm H}}}{n_{^3{\rm He}}} = 3e^{-(6\mu_B-\mu_S)/T} \tag{5.4}$$

In the model like in the data the He^3 and $\overline{He^3}$ yields have been corrected for the part coming from hypertriton and antihypertriton decays assuming a decay branch ratio for the decay of 25 %.

5.2 Predictions for RHIC and LHC

In Fig. 8 we compare p-p and heavy ion collisions at $\sqrt{s} = 200$ GeV. The difference between the two colliding systems and the effect of canonical suppression is seen in p-p collisions.

In Fig. 7 a comparison is shown of the various antiparticle/partcle ratios for two different beam energies.

The expectations for the LHC are shown in Fig. 10.

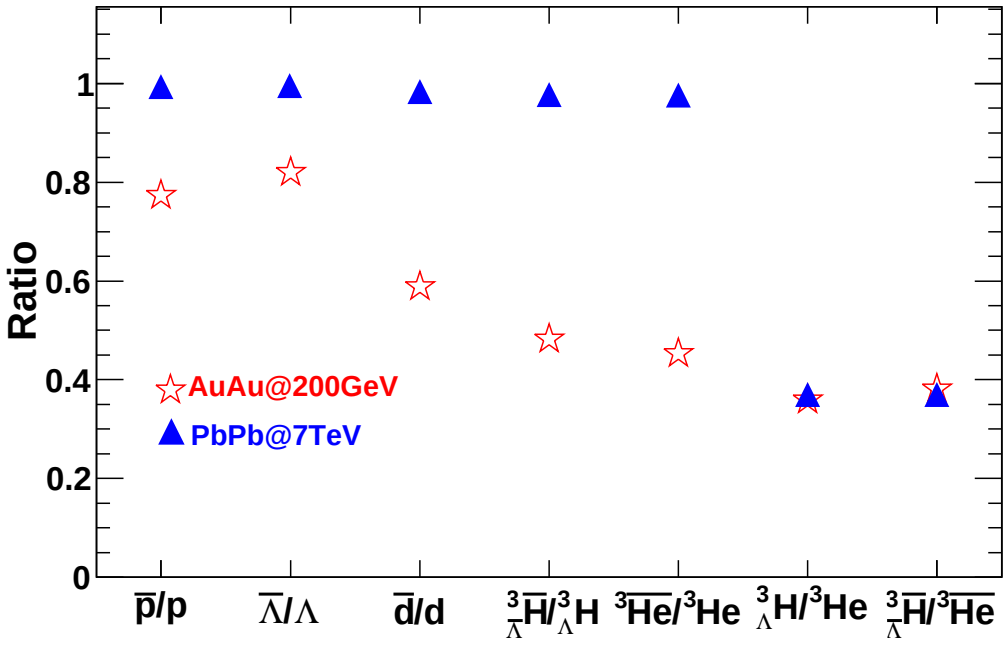

Figure 9: Comparison of two different collision energies for heavy ion collisions

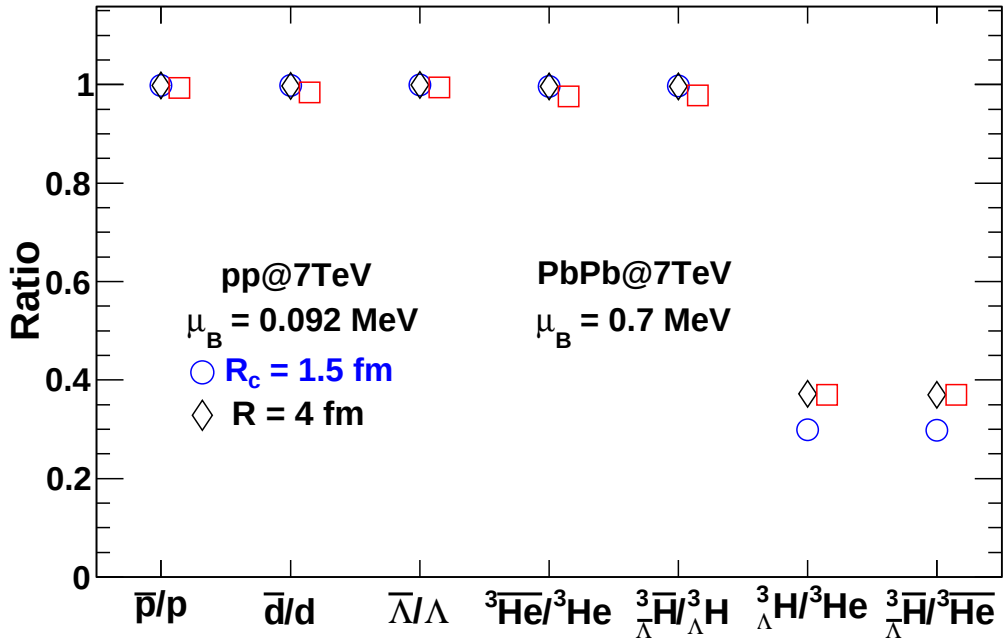

Figure 10: Prediction for $\sqrt{s}$ = 7 TeV both for pp and PbPb collision.

Finally the predictions of the thermal model for ratios of anti-nuclear to nuclear fragments are shown in Fig. 11. This figure includes comparisons for strange nuclear fragments where a clear picture emerges (again) between strange and non-strange fragments.

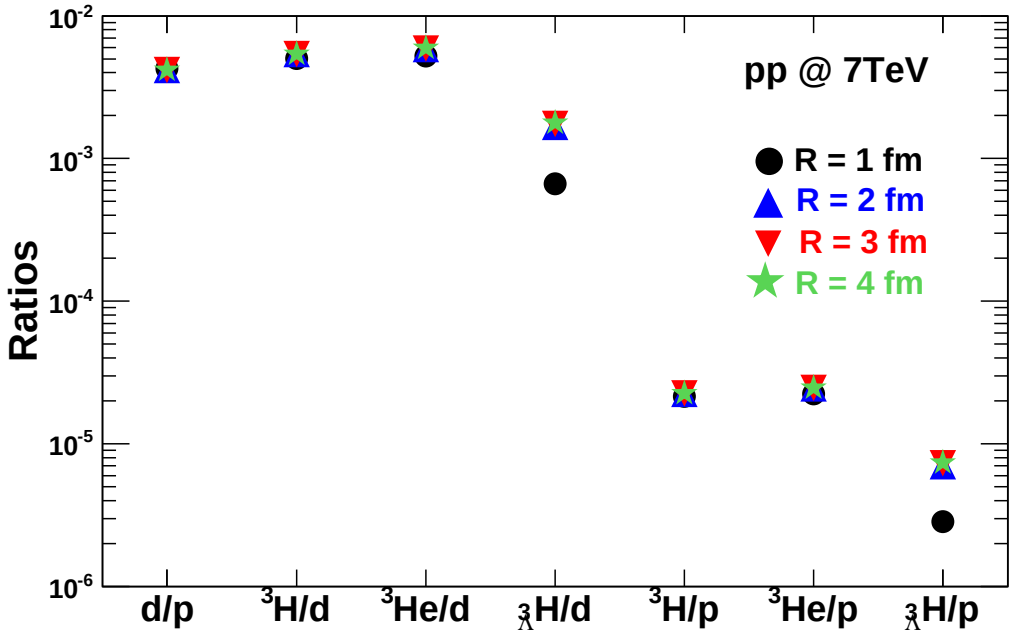

Figure 11: The ratio of the yield for examples of different masses.

6. Discussion and Summary

In the present paper we have made a general comparison of thermal parameters in p-p and heavy ion collisions. We have determined the energy dependence of the baryon chemical potential $\mu_B$in p-p collisions. This was used to establish a hierarchy of antibaryon to baryon ratios including strange and multi-strange baryons. This was then used to compare nuclear and anti-nuclear fragments in p-p and heavy ion collisions. Predictions have been presented for these ratios at LHC energies.

Acknowledgments

We acknowledge the support of DFG, the Polish Ministry of Science MEN, the CNRS, IN2P3 (France) and the Alexander von Humboldt Foundation. The financial support of the BMBF, the DFG-NRF, the Department of Science and Technology of the Government of India and the South Africa - Poland scientific collaborations are also gratefully acknowledged.

References

[1] A. Andronic, P. Braun-Munzinger, J. Stachel, e-Print: arXiv:0911.4931 [nucl-th].

[2] F. Becattini, J. Mannninen, M. Gazdzicki, Phys. Rev. C73 (2006) 044905.

[3] J. Cleymans, H. Oeschler, K. Redlich, S. Wheaton Phys. Rev. C73 034905 (2006)

[4] R. Picha, U of Davis, Ph.D. thesis 2002

[5] J. Takahashi and R. Souza for the STAR Collaboration, e-Print: arXiv:0812.415[nucl-ex], Journal of Physics G 36 (2009) .

[6] T. Galatyuk et al. (HADES collaboration, e-Print: arXiv:0911.2411[nucl-ex].

[7] N. Herrmann for the FOPI collaboration, Progr. Part. Nucl. Phys. 62 (2009) 445.

[8] J. Randrup, J. Cleymans, Phys. Rev. C74 047901 (2006).

[9] J. Randrup, J. Cleymans, e-Print: arXiv:0905.2814 [nucl-th]

[10] J. Cleymans, H. Oeschler, K. Redlich and S. Wheaton, Physics Letters B615 (2005) 50-54.

[11] B. I. Abelev *et al.* [STAR Collaboration], Phys. Rev. C **79**, 034909 (2009) [arXiv:0808.2041 [nucl-ex]].

[12] ALICE Collaboration, K. Aamodt et al., Phys. Rev. Letters **106**, 072002 (2010); e-print: arXiv:1006.5432 [hep-ex].

[13] M. Danysz and J. Pniewski, Phil. Mag. **44**, 348 (1953).

[14] D. Hahn, H. Stöcker, Nucl. Phys. A **476** (1988).

[15] H. Stöcker, W. Greiner, Phys. Rept. **137** (1986) 277.

[16] STAR Collaboration, B.I. Abelev et al., Science **328**, 58 (2010); e-print arXiv:1003.2030 [nucl-ex].

[17] R. Rapp and E.V. Shuryak, Phys. Rev. Lett. **86** (2001) 2980; e-print arXiv:hep-ph/0008326v32.

[18] E.Fermi, Prog. Theor. Phys. **5**(1950) 570; Phys. Rev. **92** (1953) 452.

[19] I. Ya. Pomeranchuk, Izv. Dokl. Akad. Nauk Ser.Fiz. **78** (1951) 889.

[20] W. Heisenberg, Naturwissenschaften **39** (1952) 69.

[21] L.D. Landau, Izv. Akad. Nauk Ser. Fiz. **17** (1953) 51.

[22] R. Hagedorn, Supplemento al Nuovo Cimento **III** (1965) 147;
R. Hagedorn, Nuovo Cimento **35**, (1965);
R. Hagedorn, Nuovo Cimento A **56** (1968) 1027.

[23] For general reviews see e.g. K. Redlich, J. Cleymans, H. Oeschler and A. Tounsi, Acta Physica Polonica B33 (2002) 1609; P. Braun-Munzinger, K. Redlich, and J. Stachel, nucl-th/0304013, invited review in Quark Gluon Plasma 3, eds. R.C. Hwa and X.N. Wang, (World Scientific Publishing, 2004).

[24] P. Braun-Munzinger, J. Cleymans, H. Oeschler and K. Redlich
Nuclear Physics A **697** (2002) 902.

[25] S. Wheaton, J. Cleymans, J. of Physics G **31** (2005) S1069, hep-ph/041203

[26] S. Wheaton, J. Cleymans, M. Hauer, Computer Physics Communications, **180** (2009) 84.

[27] A. Andronic, P. Braun-Munzinger, J. Stachel, H. Stöcker, S., arXiv:nucl-th/1010.2995v1.

[28] C. Alt *et al.* [NA49 Collaboration], arXiv:nucl-ex/0512033.

[29] C. Alt *et al.* [NA49 Collaboration], Phys. Rev. C **77**, 024903 (2008) [arXiv:0710.0118 [nucl-ex]].

[30] B. I. Abelev *et al.* [STAR Collaboration], Phys. Rev. C **75** (2007) 064901 [arXiv:nucl-ex/0607033].

[31] J. Cleymans, H. Oeschler, K. Redlich and S. Wheaton, Phys. Rev. C **73**, (2006) 034905; e-print arXiv: 0511094 [hep-ph].

[32] P. Braun-Munzinger, K. Redlich, J. Stachel, nucl-th/0304013.

[33] A.Andronic, P. Braun-Munzinger, J. Stachel Nucl. Phys. A **772** 167 (2006).